CHAPTER 6: FUEL-AIR MIXING AND COMBUSTION IN SCRAMJETS

J. Philip Drummond and Glenn S. Diskin
NASA Langley Research Center, Hampton, Virginia
j.p.drummond@larc.nasa.gov, g.s.diskin@larc.nasa.gov

Andrew D. Cutler
The George Washington University
Joint Institute for Advancement of Flight Sciences, Hampton, Virginia
a.d.cutler@larc.nasa.gov

6.1 Introduction

At flight speeds, the residence time for atmospheric air ingested into a scramjet inlet and exiting from the engine nozzle is on the order of a millisecond. Therefore, fuel injected into the air must efficiently mix within tens of microseconds and react to release its energy in the combustor. The overall combustion process should be mixing controlled to provide a stable operating environment; in reality, however, combustion in the upstream portion of the combustor, particularly at higher Mach numbers, is kinetically controlled where ignition delay times are on the same order as the fluid scale. Both mixing and combustion time scales must be considered in a detailed study of mixing and reaction in a scramjet to understand the flow processes and to ultimately achieve a successful design.

Although the geometric configuration of a scramjet is relatively simple compared to a turbomachinery design, the flow physics associated with the simultaneous injection of fuel from multiple injector configurations, and the mixing and combustion of that fuel downstream of the injectors is still quite complex. For this reason, many researchers have considered the more tractable problem of a spatially developing, primarily supersonic, chemically reacting mixing layer or jet that relaxes only the complexities introduced by engine geometry. All of the difficulties introduced by the fluid mechanics, combustion chemistry, and interactions between these phenomena can be retained in the reacting mixing layer, making it an ideal problem for the detailed study of supersonic reacting flow in a scramjet. With a good understanding of the physics of the scramjet internal flowfield, the designer can then return to the actual scramjet geometry with this knowledge and apply engineering design tools that more properly account for the complex physics. This approach will guide the discussion in the remainder of this section.

6.2 Reacting Mixing Layers and Jets

As described earlier, compressible shear/mixing layers and jets provide good model problems for studying the physical processes occurring in high-speed mixing and reacting flow in a scramjet. Mixing layers are characterized by large-scale eddies that form due to the high shear that is present between the fuel and air streams. These eddies entrain fuel and air into the mixing region. Stretching occurs in the interfacial region between the fluids leading to increased surface area and locally steep concentration gradients. Molecular diffusion then occurs across the strained interfaces. There has been a significant amount of experimental and numerical research to study mixing layer and jet flows [1]- [9]. For the same velocity and density ratios between fuel and air, increased compressibility, to the levels present in a scramjet, results in reduced mixing layer growth rates and reduced mixing. The level of compressibility in a mixing layer with air stream 1 and fuel stream 2 can be approximately characterized by the velocity ratio, $r = U_2/U_1$, the density ratio,

s $= \rho_2/\rho_1$, and the convective Mach number, $M_c = (U_2 - U_1)/(a_1 + a_2)$ where a is the speed of sound. Increased compressibility reorganizes the turbulence field and modifies the development of turbulent structures. The resulting suppressed transverse Reynolds normal stresses appear to result in reduced momentum transport. In addition, the primary Reynolds shear stresses responsible for mixing layer growth rate also are reduced. The primary mixing layer instability becomes three-dimensional with a convective Mach number above 0.5, reducing the growth of the large scale eddies. Finally, the turbulent eddies become skewed, flat, and less organized as compressibility increases. All of these effects combine to reduce the growth rate of the mixing layer and the overall level of mixing that is achieved.

Several phenomena result in the reduction of mixing with increasing flow velocity, including the velocity differential between fuel and air, and compressibility. Potentially, the existence of both high and low growth and mixing rates are possible, and the engine designer with an understanding of the flow physics controlling these phenomena can advantageously use these effects. The shock and expansion wave structure in and about the mixing layer can interact with the turbulence field to affect mixing layer growth [1]. Shock and expansion waves interacting with the layer result from the engine internal structure. Experiments have shown that the shocks that would result from wall and strut compressions appear to enhance the growth of the two-dimensional eddy structure (rollers) of a mixing layer. This effect is most pronounced when the duct height in the experiment and the shear layer width become comparable. Waves may be produced by the mixing layer itself under appropriate conditions. Localized shocks (often termed shocklets) occur within the mixing layer when the accelerating flow over an eddy becomes supersonic even when the surrounding flow is subsonic. When the overall flow is supersonic, the eddy shocklets will extend as shocks into the flow beyond the individual eddies. These shocklets can retard eddy growth due to increased localized pressure around the eddy.

The growth of a mixing layer produces a displacement effect on the surrounding flow field. This displacement in confined flow produces pressure gradients that can affect the later development of the mixing layer, typically retarding growth. When chemical reaction occurs in a mixing layer, resulting in heat release, the growth of the mixing layer is retarded in both subsonic and supersonic flow [1, 2]. The effect of heat release can also vary spatially as a function of the local stoichiometry and chemical reaction. The retarded growth in both instances can be reversed, however, by allowing the bounding wall to diverge relative to the initial wall angles where retarded growth was noted [1]. While the process of mixing layer growth is affected by the combustor geometry and design, fuel injector design carried out with proper consideration for the inlet and combustor geometry can have a strong influence on overall mixing and combustion efficiency. Considerable effort has been expended over the past fifteen years to achieve efficient fuel injector designs. Injector design will be considered in the next section.

6.3   Scramjet Fuel Injectors

There are several key issues that must be considered in the design of an efficient fuel injector. Of particular importance are the total pressure losses created by the injector and the injection processes, that must be minimized since the losses reduce the thrust of the engine. The injector design also must produce rapid mixing and combustion of the fuel and air. Rapid mixing and combustion allow the combustor length and weight to be minimized, and they provide the heat release for conversion to thrust by the engine nozzle. The fuel injector distribution in the engine also should result in as uniform a combustor profile as possible entering the nozzle so as to produce an efficient nozzle expansion process. At moderate flight Mach numbers, up to Mach 10, fuel injection may have a normal component into the flow from the inlet, but at higher Mach numbers, the injection must be nearly axial since the fuel momentum provides a significant portion of the engine thrust. Intrusive injection devices can provide good fuel dispersal into the surrounding air, but they require active cooling of the injector structure. The injector design and the flow disturbances produced by injection also should provide a region for flameholding, resulting in a stable piloting source for downstream ignition of the fuel. The injector cannot result in too severe a local flow disturbance, that could result in locally high wall static pressures and temperatures, leading to increased frictional losses and severe wall cooling requirements.

A number of options are available for injecting fuel and enhancing the mixing of the fuel and air in

high-speed flows typical of those found in a scramjet combustor [10, 11]. Two traditional approaches for injecting fuel include injection from the combustor walls and in-stream injection from struts. The simplest approach for wall injection involves the transverse injection of the fuel from wall orifices. Transverse injectors offer relatively rapid near-field mixing and good fuel penetration. Penetration of the fuel stream into the cross-flow is governed by the jet-to-freestream momentum flux ratio. The fuel jet interacts strongly with the cross-flow, producing a bow shock and a localized highly three-dimensional flow field. Resulting upstream and downstream wall flow separations also provide regions for radical production and flameholding, but they can also result in locally high wall heat transfer. Compressibility effects that were noted earlier for mixing layer flows also are evident in the mixing regime downstream of a transverse jet. Compressibility again retards eddy growth and breakup in the mixing layer and suppresses entrainment of fuel and air, resulting in a reduction in mixing and reaction.

Improved mixing has also been achieved using alternative wall injector designs. Wall injection using geometrical shapes that introduce axial vorticity into the flow field has been successful. Vorticity can be induced into the fuel stream using convoluted surfaces or small tabs at the exit of the fuel injector. Alternatively, vorticity can be introduced into the air upstream of the injector using wedge shaped bodies placed on the combustor walls. Vorticity addition to the air stream provides more significant mixing enhancement of fuel and air [12]. When strong pressure gradients are present in the flowfield, e.g. at a shock, vorticity aligned with the flow can be induced at a fuel-air interface, where a strong density gradient exists, by virtue of the baroclinic torque. Fuel injection ramps have proven to be an effective means for fuel injection in a scramjet engine [2]. Fuel is injected from the base of the ramp. The unswept ramp configuration provides nearly streamwise injection of fuel to produce a thrust component. The effects of angled injection on axial thrust only go as the cosine of the angle, so small injection angles result in little loss in thrust. Flow separation at the base of the ramp provides a region for flame holding and flame stabilization through the buildup of a radical pool. The ramp itself produces streamwise vorticity as the air stream sheds off of its edges, improving the downstream mixing. The swept ramp design provides all of the features of the unswept ramp, but the sweep results in better axial vorticity generation and mixing. A novel variation on the swept wedge injector, termed the aero-ramp injector [13], utilizes three arrays of injector nozzles at various inclination and yaw angles to approximate the physical swept ramp design.

In-stream injection also has been utilized for fuel injection in a scramjet. Traditional approaches involve fuel injection from the sides and the base of an in-stream strut. Transverse injection results in behavior similar to transverse fueling from the wall, although differences can occur due to much thinner boundary layers on the strut. Injection from the base of the strut results in slower mixing as compared to transverse injection. A combination of transverse and streamwise injection, varied over the flight Mach number range, often has been utilized to control reaction and heat release in a scramjet combustor. As noted earlier, however, streamwise injection has the advantage of adding to the thrust component of the engine. To increase the mixing from streamwise injectors, many of the approaches used to improve wall injection, including non-circular orifices, tabs, and ramps, have been successfully utilized. Several new concepts have emerged as well. Pulsed injection using either mechanical devices or fluidic oscillation techniques have shown promise for improved mixing. Pulsed injection of fuel utilizing a shuttering technique to control injection has been shown to improve mixing [12]. Fuel injection schemes integrated with cavities also provide the potential for improved mixing and flameholding. This type of integrated fuel injection/flameholding device, utilizing fuel injection into a cavity and from its base, integrates the fuel injection with a cavity that provides flameholding, flame stabilization, and mixing enhancement if the cavity is properly tuned. Air exchange rates with the cavity may be low, however, limiting the amount of fuel that can be added. Additional scramjet fuel injector designs continue to be introduced and studied to achieve even higher levels of mixing and combustion efficiency.

Scramjet design is built upon both experimental and computational research. To assure that computational tools properly represent the complex flow physics in a scramjet, careful evaluation of the computational tools is necessary. Benchmark experiments are becoming available that provide the necessary data for evaluating the accuracy of the numerical algorithms and the physical models that the computational tools employ. In addition, these experiments provide in some instances the information necessary to improve the modeling employed by the codes. Two experiments available for assessing high-speed combustion codes are described in the next section. Results obtained from the application of a combustion code to these experiments are also shown and discussed.
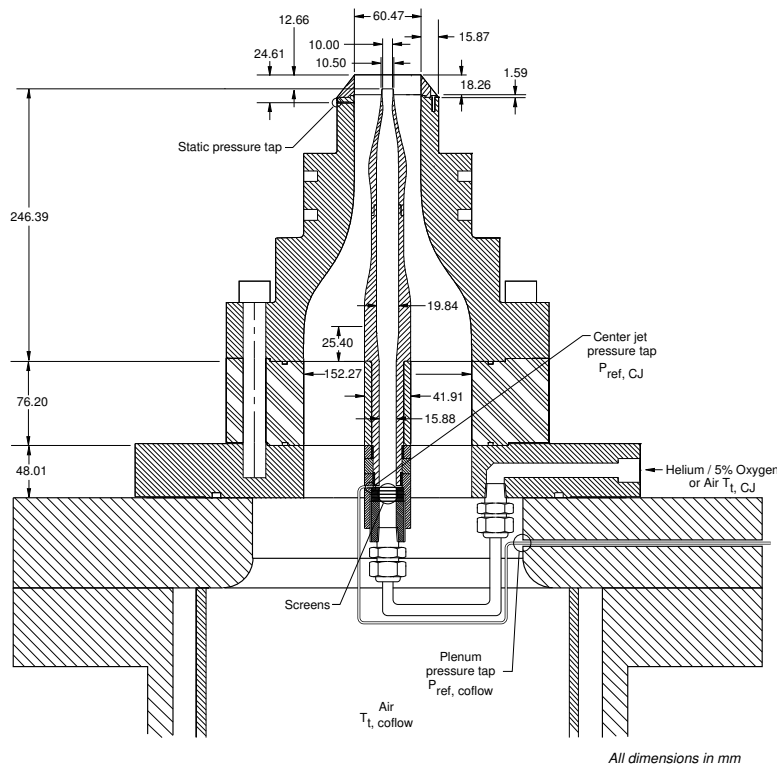
Figure 1: Coaxial jet assembly cross-section

6.4   Mixing and Combustion Experiments

Two basic experiments are being conducted at the NASA Langley Research Center to collect detailed high-speed mixing and combustion data for use in physical model development and code validation. The first experiment concerns coaxial jet mixing of a helium/oxygen center jet with a coflowing air outer jet and was chosen to provide detailed supersonic mixing data. The second experiment was developed to study high-speed mixing and combustion in a simple "scramjet like" engine environment. The experiment utilizes a ducted flow rig containing vitiated supersonic air with a single fuel injector that introduces supersonic gaseous hydrogen from the lower wall. Detailed wall and in flow surveys and noninterference diagnostics are used in both experiments. These experiments will be described in the following sections.

6.4.1   Coaxial Jet Mixing Experiment

A coaxial jet mixing experiment has been developed to study the high-speed compressible mixing of helium and air. Details of the experiment are described in references [14] and [15]. The low-density helium, which serves as a simulant of hydrogen fuel, was chosen to allow detailed studies of mixing without chemical reaction. Oxygen is added to the helium jet as a diagnostic aid for an oxygen flow-tagging technique (RELIEF). Several methods are utilized to characterize the flow field including Schlieren visualization, pitot pressure, total temperature, and gas sampling probe surveying, and RELIEF velocimetry. A schematic of the coaxial jet configuration is shown in Figure 1. The rig consists of a 10 mm inner nozzle from which helium, mixed with 5 percent oxygen by volume, is injected at Mach 1.8 and an outer nozzle 60 mm in diameter from which coflowing air is introduced also at Mach 1.8. The velocity ratio between the two jets is 2.25, the convective Mach number is 0.7, and the jet exit pressures are matched to one atmosphere.

The resulting flow downstream of the nozzles can be seen in Figure 2, which shows a Schlieren image of the flowfield. The development of the mixing layer between the central helium jet and the air jet can be
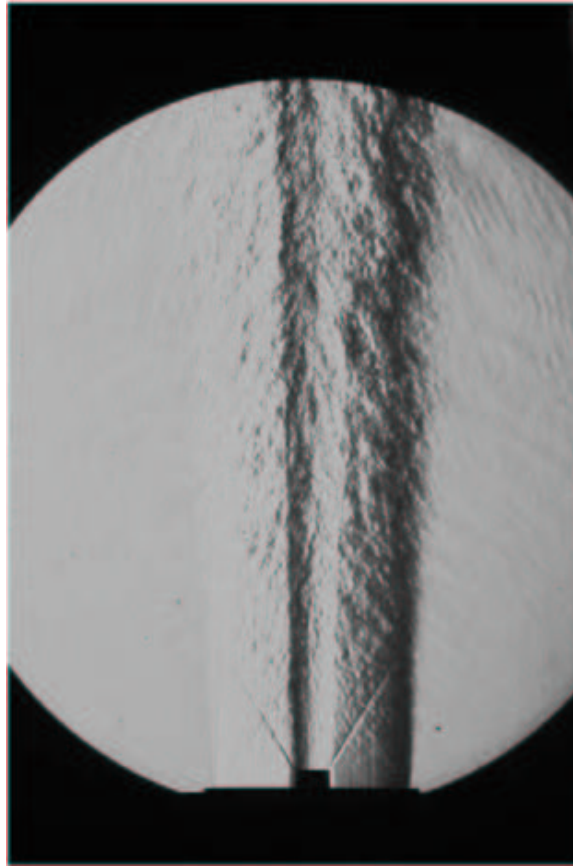
Figure 2: Schlieren image of coaxial jet mixing (conical extension cap removed)

seen along with the shear layer development between the air jet and the surrounding quiescent laboratory air into which the air jet exhausts. Shock-expansion wave structure emanating outward from the centerbody nozzle lip can also be seen. Inward propagating waves from the inner lip, due to the finite thickness of the lip (0.25 mm), can be observed in the air jet once they pass through the helium jet. These waves are not visible in the helium jet due to the low refractive index within the center jet. A third wave can also be observed emanating inward from the outer nozzle lip and traversing both the air jet and the helium jet. Additional results from the experiment will also be considered later in this section when comparisons of the measured data with numerical simulations are made.

6.4.2 SCHOLAR Combustor Experiment

A direct-connect supersonic combustor model, known by its acronym SCHOLAR, has been developed for testing in a combustion heated test facility at the NASA Langley Research Center. This experiment has been designed to provide optical access to a reacting supersonic flowfield typical of the flow present in a scramjet engine. Details of the experiment are described in reference [16]. The model shown in Figure 3a consists of a section 546 mm in length constructed of copper for thermal control followed by a 914 mm long section of carbon steel attached to the aft end of the copper section. The copper section contains a single fuel injector that introduces gaseous hydrogen into the vitiated air stream flowing through the model.

The injector region of the combustor model is shown in Figure 3b. The model consists of a constant area channel initially 38.6 mm high and 87.9 mm wide followed by a 4.8 mm rearward-facing step and a 43.8 mm long constant area section. Combustion heated vitiated air is introduced into the channel at
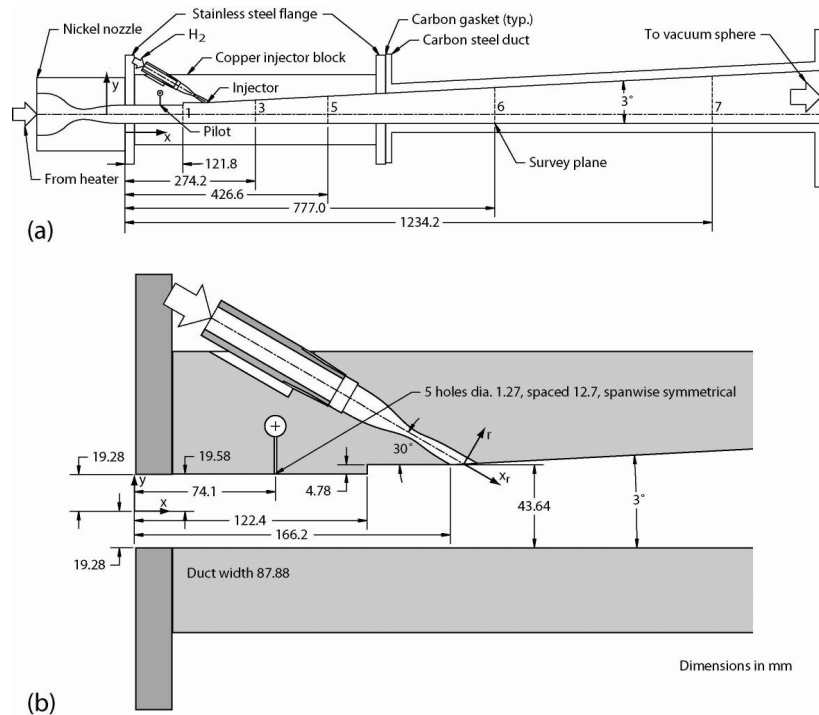
Figure 3: SCHOLAR combustor model: (a) nozzle, copper and steel duct sections; (b) detail near fuel injector and pilots.

Mach 2, 1184 K, and 100405 Pa. The vitiated air contains 20.35 percent water by mass introduced by the facility heater. A small amount of hydrogen fuel at a fuel equivalence ratio of 0.15 is introduced downstream from five pilot injectors along the upper wall at the 74.1 mm station. Each pilot injector is 1.27 mm in diameter. The central pilot injector lies on the duct centerline, and the remaining four injectors are spaced 12.7 mm from one another on either side of the central jet. This fuel is used to pilot the primary Mach 2.5 hydrogen fuel injector further downstream at the 173.2 mm station by igniting and producing a radical pool to enhance ignition of the primary fuel-air mixture. The primary fuel injector is inclined at 30 degrees to the horizontal and has a circular cross-section 7.6 mm in diameter. A 3 degree expansion of the upper wall begins immediately at the primary fuel injector. This 3 degree expansion continues along the upper wall of the carbon steel section that is attached to the copper model.

Five measurement locations for optical access are provided in the copper section of the model. Two additional measurement stations are provided in the carbon steel section. The measurement stations indicated in Figure 3a are slits in both model side walls, through which planar BOXCARS measurement beams enter and exit, allowing single-shot measurements to be made of static temperature (ro-vibrational temperature of N_2 molecules). These measurements are single point measurements, but the location of the measurement is translated during the tests to provide a full plane of data at each station. From these single-shot measurements, averages and RMS values are derived. In additional to optical measurements, wall pressures are measured using an array of orifices.

6.5   Simulation of Mixing and Combustion Experiments

The mixing and combustion experiments described earlier were numerically simulated before data was collected to assist in the experimental design. Additional simulations were also performed during and following the experimental study to compare with the measured data. Initial simulations were made with the SPARK combustion code. Additional studies with other combustion codes are being conducted [15]. Details on the
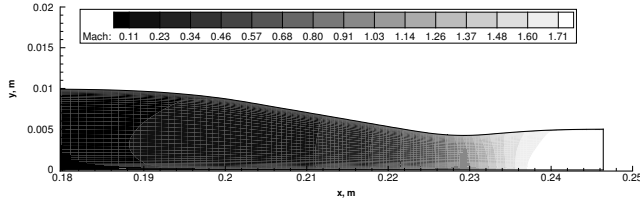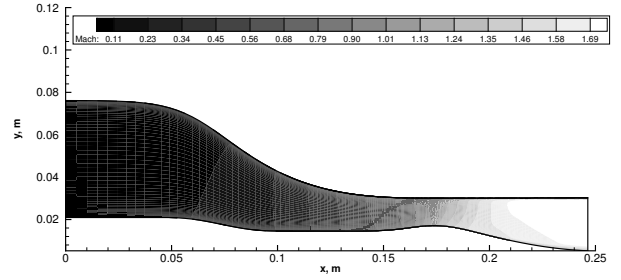
Figure 4: Mach contours in inner nozzle

Figure 5: Mach contours in outer nozzle

simulations of both experiments and comparisons with measured data are given in the following sections.

6.6 Simulations of the Coaxial Jet Mixing Experiment

The axisymmetric version of the SPARK code was used to simulate the flowfield in the helium/oxygen center nozzle and the outer air nozzle of the coaxial jet experiment. Details of the code are given in reference [17]. This version of the code solves the axisymmetric full Navier-Stokes equations and species continuity equations describing the production, convection, and mixing of each relevant species. The analysis of the experiment was begun by first solving for the flowfield in the center and outer nozzles using the nozzle contours specified in the last section. The domain of the inner nozzle was discretized with a grid of 201 points in the streamwise direction and 51 points in the radial direction. The domain of the outer nozzle was discretized with a grid of 201 points in the streamwise direction and 101 points in the radial direction. Initial conditions in the subsonic portions of the nozzles were specified at the x = 76.2 mm station. For the inner nozzle at this station, the streamwise velocity was 141.8 m/s, the static temperature was 297.4 K, and the static pressure was 614300 Pa. The helium mass fraction in the inner jet was 0.6995 and the oxygen mass fraction was 0.3005. In the outer nozzle at the 76.2 mm station, the streamwise velocity, static temperature and pressure of the air were 22.94 m/s, 299.74 K, and 578100 Pa, respectively. No slip conditions were specified along the nozzle walls and first order extrapolation was used at the supersonic outflow station of each nozzle. Symmetry conditions were specified along the centerline of the inner nozzle. Turbulence in the outer nozzle was modeled using a Cebeci-Smith model. The flow in the inner nozzle was assumed to be laminar consistent with the behavior observed in the experiment at the outflow of the nozzle. Results from the center and outer nozzle simulations detailing Mach number distributions are given in Figures 4 and 5, respectively. The initial station (x = 76.2 mm) of both nozzles is reset to zero in the calculations. The Mach number ranges from a minimum of 0.1 in the subsonic portion of the nozzles to a maximum of 1.8 at the end of each nozzle. As can be seen from the figures, both nozzles produce very uniform exit flow fields resulting in ideal initial conditions for the mixing study in the region downstream of the nozzle exits.

Results obtained at the end of each nozzle were then used to specify the supersonic inflow conditions for the downstream domain beyond the nozzles where mixing of the jets occurred. The downstream domain was 150 mm long. The upper boundary of the domain was specified at y = 30.24 mm to coincide with the end of the outer nozzle wall. Radially beyond this point, laboratory air is entrained by the outer jet, but measurements have shown relatively low streamwise velocities of only a few meters per second in the entrained flow. Later measurements are planned to confirm these conditions. It is not appropriate to simulate such a low speed flow with a compressible code, so a slip boundary was chosen at y = 30.24 mm so as to consider only the compressible regime. Large scale structure certainly forms at this interface as the two streams viscously interact. Waves from this structure reach the helium-air interface near the nozzle exit. However, the air coflow-ambient air mixing layer does not start to merge with the helium-air mixing layer until the end of the experimental domain. The domain was discretized with a grid of 401 points in the streamwise direction and 201 points in the radial direction. The grid was radially compressed in the region of the helium-air mixing layer. Symmetry boundary conditions were specified along the y = 0 boundary and slip conditions were specified along the upper boundary at y = 30.24 mm. The outflow boundary at x =
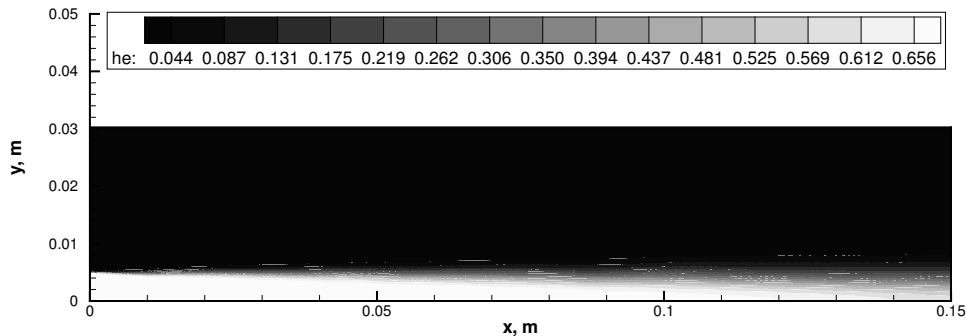
Figure 6: Helium mass fraction contours downstream of nozzles

150 mm remained supersonic, and extrapolation conditions were specified at this location. Turbulence was modeled in the downstream domain with the turbulent jet mixing model of Eggers and Eklund [18, 19].

Results from the downstream calculation are shown in Figures 6 through 8. Helium-air mixing downstream of the nozzles is shown in Figure 6. The helium mass fraction in the figure ranges from a minimum of zero to a maximum of approximately 0.7. There is significant mixing of the helium and air throughout the downstream region although relatively high mass fractions of helium still remain near the centerline.

A comparison of the measured helium mass fraction data with the simulation results at several stations downstream of the nozzles is given in Figure 7. Agreement between the simulation and the data is very good at each station. The code somewhat overpredicts the mixing near the centerline at the x = 0.12 m station, although the prediction improves with increasing radial distance. A comparison of measured pitot pressures with the simulation is shown in Figure 8. Agreement is good in the region of the air coflowing jet, but the simulation somewhat overpredicts the pitot pressure in the helium-air mixing region. The comparison with the experimental data differs at large radial distances greater than 0.025 m as the code does not consider the effects of the laboratory air entrained by the coaxial air jet. The RELIEF streamwise velocity data is compared with the simulation in Figure 9. The prediction agrees well with the data at the first three stations and slightly overpredicts the data at the remaining stations near the centerline. The simulation somewhat underpredicts the the velocity at the final three stations in the mixing region between the helium and air coflowing jets in agreement with the pitot pressure results.

6.6.1 Simulations of the SCHOLAR Combustor Experiment

The three-dimensional version of the SPARK code was used to simulate the flowfield in the SCHOLAR combustor model. Details of the code are given in the references [17, 20]. This version of the code solves the 3-D full Navier-Stokes equations and species continuity equations describing the production, convection, and mixing of chemical species. Calculations have been used in the design and refinement of the experiment. In the calculation the model was rotated from the orientation shown in Figure 3 such that the injector wall was aligned with the lower computational boundary.

Calculations were begun at the x = 0 station of the SCHOLAR model where vitiated air from the facility enters the duct. Vitiated air entered the model at Mach 2.0 yielding a velocity of 1395.7 m/s, a static temperature of 1184 K, and a static pressure of 100405 Pa. The calculated equilibrium mole fractions of the species present in the vitiated air, determined by a quasi-one-dimensional nozzle code, are given in Table 1.

The initial channel cross-section is 38.6 mm high and 87.9 mm wide. The hydrogen fuel injector introduces
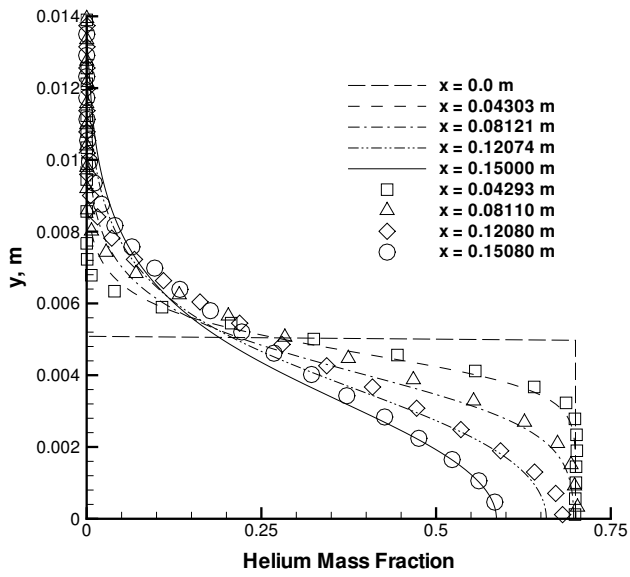
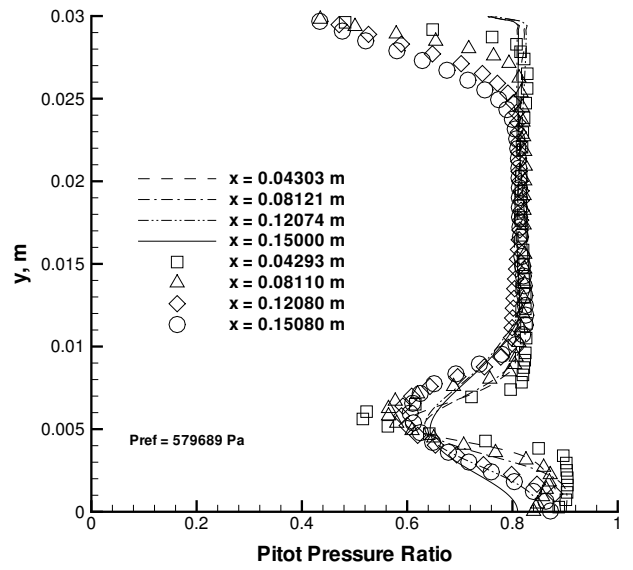Figure 7: Comparison of helium mass fraction data with simulation results

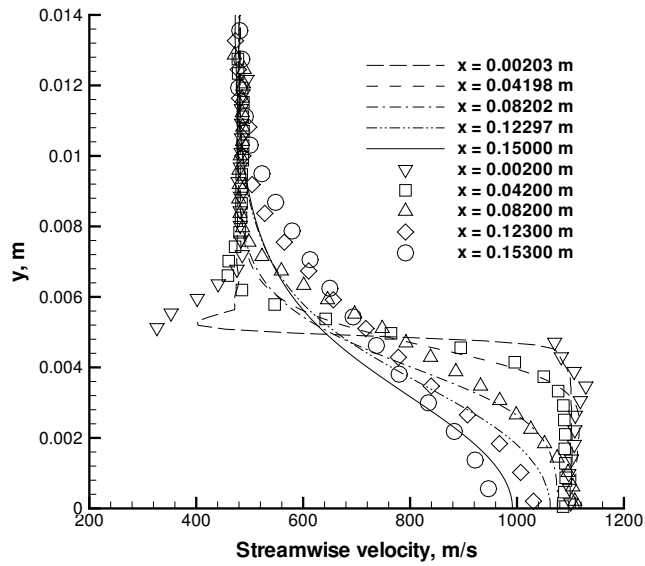Figure 8: Comparison of pitot pressure data with simulation results

Figure 9: Comparison of RELIEF velocity data with simulation results

Species	Mole Fraction	Species	Mole Fraction
H	6.00000×10^{-08}	O	4.00000×10^{-06}
OH	2.43910×10^{-04}	O_2	1.86499×10^{-01}
HO_2	9.80000×10^{-07}	CO	1.00873×10^{-11}
H_2	2.86000×10^{-06}	CO_2	2.24589×10^{-04}
H_2O	2.92619×10^{-01}	Ar	6.32850×10^{-03}
H_2O_2	2.98644×10^{-09}	HCO	1.26462×10^{-24}
HNO	3.80338×10^{-12}	H_2CO	9.04513×10^{-26}
N	3.70036×10^{-18}	CH_3	4.27856×10^{-40}
N_2	5.12668×10^{-01}	CH_4	9.20779×10^{-39}
NO	1.62088×10^{-03}	C_2H_2	0.0
NO_2	1.19100×10^{-05}	C_2H_4	0.0

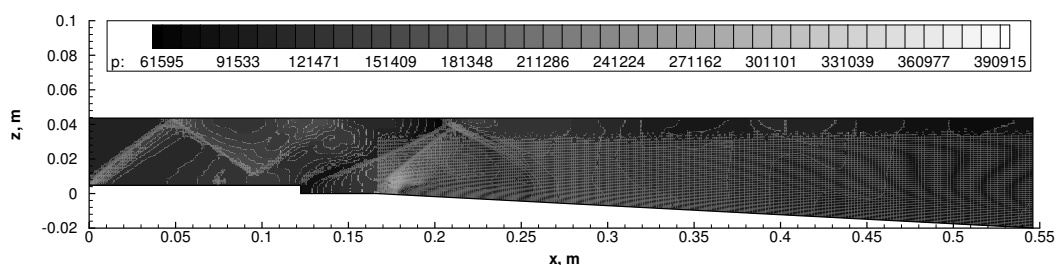Table 1: Vitiate mole fraction at test condition

Figure 10: Static pressure contours along streamwise plane

hydrogen through a choked nozzle at Mach 2.5, a static temperature of 134.2 K, and a static pressure of 201300 Pa. The pilot fuel injectors described earlier were activated to improve flameholding under the present test conditions. The pilot injectors are assumed to be choked at the wall surface, resulting in a static temperature and pressure of 251.7 K and 722535 Pa, respectively. No slip conditions were specified along the upper, lower, and near- and far-side channel walls. First order extrapolation was used at the supersonic outflow station located at the 546 mm station for this calculation. This domain was discretized with a grid of 401 points in the streamwise direction, 61 points in the cross-stream direction, and 121 points in the spanwise direction. The grid was compressed near the solid walls and the fuel injector. Turbulence was modeled in the near wall region using the Bauldwin-Lomax model, and in the interior field using the turbulent jet mixing model [18, 19]. Chemistry was modeled using the 9 species, 18 reaction model described in reference [17]. This model provides a detailed description of hydrogen-air chemistry, but does not consider the effects of the small quantities of oxides of nitrogen and hydrocarbon species present in the vitiated air.

The results of flowfield simulations of the SCHOLAR combustor model are shown in Figures 10-16. Figure 10 shows static pressure contours along the streamwise plane centered on the fuel jet. Traversing the combustor from inflow to outflow, a weak bow shock produced by the pilot injectors can be seen. This pressure rise is communicated through the wall boundary layer resulting in a weak shock at the inflow to the combustor. This is followed by the expansion of the flow over the lower wall step. Just downstream, the flow is compressed through a recompression shock followed by a strong bow shock lying ahead of the primary fuel injector. Both the fuel jet and its surrounding air flow then expand beyond the fuel injector. The reflection of the bow shock interacts with the low density hydrogen fuel jet altering the shock angle. Figure 11 shows the static temperature contours along the same streamwise plane. The temperature rise associated with combustion of the pilot fuel near the primary fuel injector, and combustion of the shear layer of the primary injector plume can also be seen. Figure 12 shows the resulting Mach number contours along
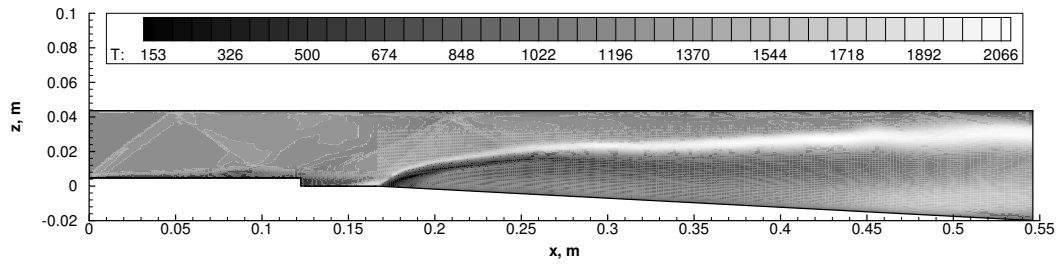
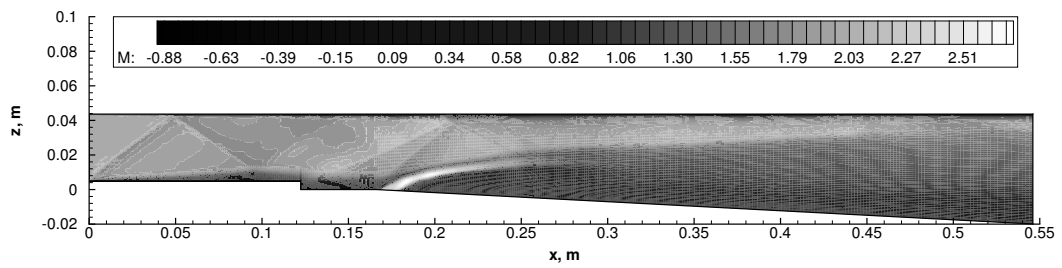Figure 11: Static temperature contours along streamwise plane

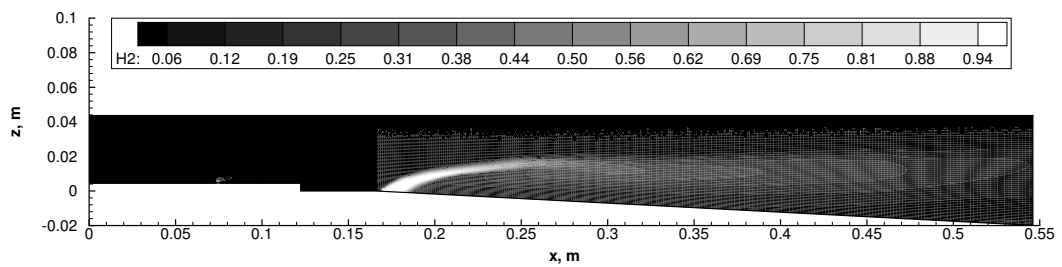Figure 12: Mach number contours along streamwise plane

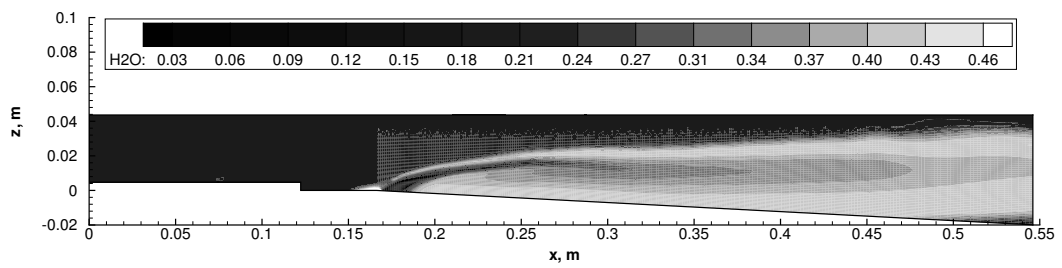Figure 13: Hydrogen mass fraction contours along streamwise plane

Figure 14: Water mass fraction contours along streamwise plane
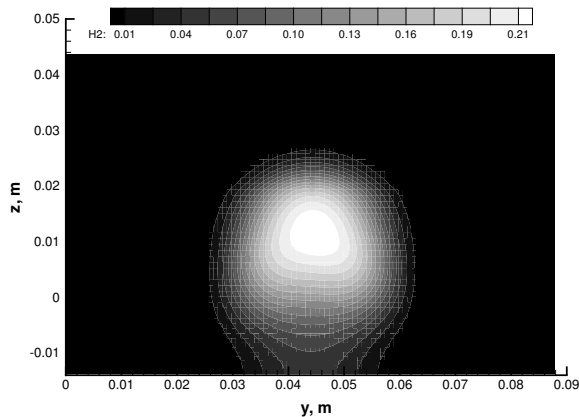
131

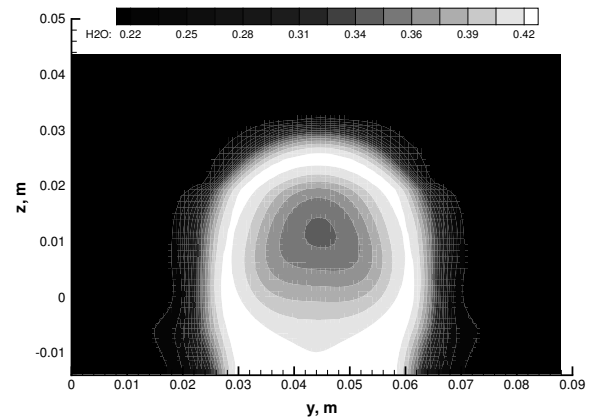Figure 15: Hydrogen mass fraction at downstream station (0.427 m)

Figure 16: Water mass fraction at downstream station (0.427 m)

the streamwise plane. In addition to the above features, the wall boundary layers can be seen along with regions of recirculation located behind the lower wall step and where the bow shock interacts with the upper wall boundary layer. The plume of the fuel jet can also be seen. Figure 13 also displays the jet in terms of mass fraction contours of hydrogen along the streamwise plane. Figure 14 shows contours of the water mass fraction produced as a result of chemical reaction of the hydrogen fuel and air. The contours range from a minimum mass fraction of zero in the hydrogen jet core to a maximum mass fraction of 0.46 including the water introduced in the air from facility vitiation.

Figures 15 and 16 show contours of hydrogen and water mass fraction, respectively, in a cross-plane at the 0.427 m station bounded by the channel walls. Values of the hydrogen mass fraction range from zero to 0.23 with the highest concentrations existing only in the immediate jet core. Significant amounts of hydrogen have been mixed with facility air and consumed downstream by reaction. Values of the water contours again range from a minimum mass fraction of 0.203 (from vitiation) to a maximum mass fraction of 0.44. Vortices that form as the facility air interacts with the fuel jet lift and spread the jet enhancing fuel-air mixing and reaction. The vortices also convect fluid toward the lower wall and into the remaining fuel jet.

Comparisons of the measured and computed static temperatures at three stations in the copper section of the SCHOLAR model are given in Figures 17 through 19. These stations correspond to stations 1, 3, and 5 in Figure 3a. Measurements were not made for the piloted runs at stations 6 and 7 in the steel section of the SCHOLAR model. Figure 17 shows results at the step in the model wall. The computed results show a rise in temperature ranging from 400K on the walls to 1299K where the pilot fuel is mixing with the facility air and heating, but not undergoing combustion. The measured data ranges from 850K to 1200K in the flow with the fuel and air mixing but not reacting. The asymmetry of the data may simply be attributed to the coarseness of the grid used in surveying the flow relative to the scale of the flow features combined with the slightly asymmetrical location of the grid with respect to the flow. There is no suggestion that the flow itself is not symmetrical. At the 0.274 m station shown in Figure 18, the data now indicate combustion of the pilot fuel whereas the computation shows combustion of the pilot fuel and initial combustion of the primary injector fuel. The computation and the data indicate a maximum temperature of around 2030K and 2300K, respectively. A "cold" core of hydrogen still persists in both the data and the calculation. Figure 19 shows results at the 0.427 m station. Further combustion of the primary injector fuel in the mixing layer between the hydrogen and the facility air is indicated in the calculation. The data indicates increased combustion and temperature rise of the pilot fuel and on the lower surface of the primary injector hydrogen-air mixing layer. No combustion of the fuel is seen in the data along the upper surface of the primary fuel jet at this location.
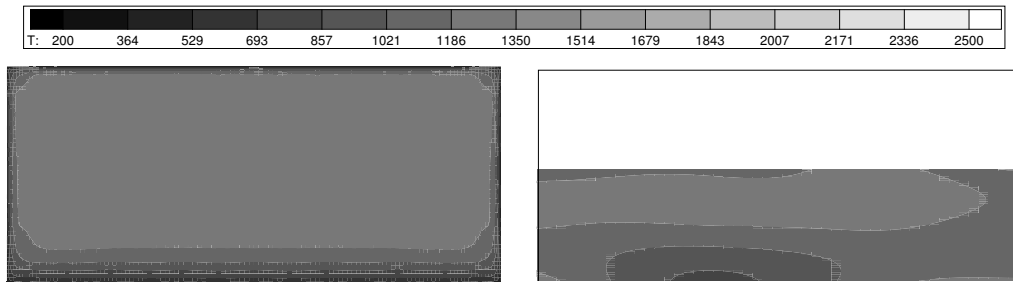
132

Figure 17: Comparison of computed static temperature (left) with data at 0.122 m station
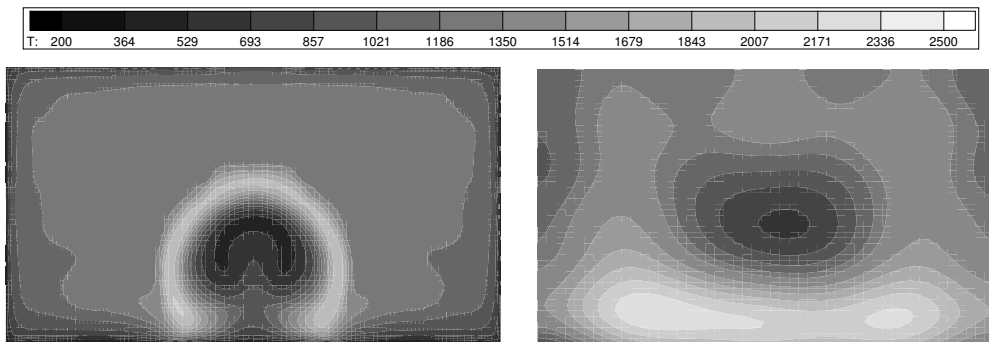

Figure 18: Comparison of computed static temperature (left) with data at 0.274 m station
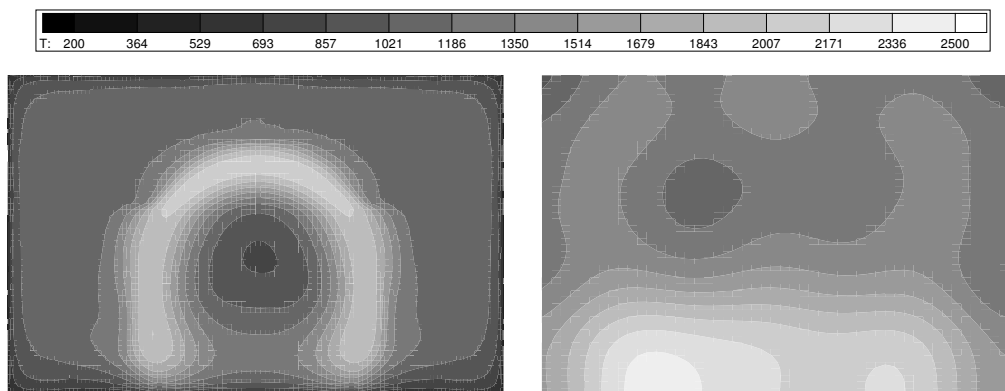

Figure 19: Comparison of computed static temperature (left) with data at 0.427 m station

6.7 Concluding Remarks

Activities in the area of scramjet fuel-air mixing and combustion associated with the Research and Technology Organization Working Group on Technologies for Propelled Hypersonic Flight have been described. Work discussed in this chapter has centered on the design of two basic experiments for studying the mixing and combustion of fuel and air in a scramjet. Simulations were conducted to aid in the design of these experiments. The experimental models were then constructed, and data were collected in the laboratory.

Comparison of the data from the non-reacting coaxial jet mixing experiment with one combustor code were then made and described. The comparisons of the helium mass fraction and pitot pressure data with the simulation were good, although there were some observed differences in the measured and computed pitot pressure in the jet mixing region.

The SCHOLAR combustor experiment flowpath was then analyzed and comparisons were made with CARS temperature data. Computed results indicate that the five pilot injectors ignite just ahead of the primary fuel injector and aid in ignition downstream of the injector. Combustion then occurs at later stations in the hydrogen-air mixing layer around the primary fuel jet. The CARS temperature data also indicates that combustion of the pilot fuel is delayed beyond the step, but occurs further downstream. Near the end of the copper section of the SCHOLAR model, increased temperature due to combustion is noted in both the computation and the data. The highest temperatures in the data (2400K) lie near the lower wall. The highest computed temperatures (2100K) lie around the upper region of the remaining fuel core at this station. Overall, the computation exhibits more significant combustion of the primary fuel jet relative to the degree of combustion indicated by the CARS temperature data.

It is hoped that combustion codes currently employed in scramjet design will be used to simulate both experiments and to compare results with the experimental data. Further discussion of the experiments is given in Chapter 7. Data from the coaxial jet experiment and the SCHOLAR experiment have been made available on the web for the use of other researchers. Shared experiences from the simulations should be very useful in improving the capabilities of each of the codes and the models that these codes employ.

References

[1] Dimotakis, P. E., Turbulent Free Shear Layer Mixing and Combustion. High Speed Flight Propulsion Systems, Chapter 7, Progress in Astronautics and Aeronautics, Vol. 137, 1991.

[2] Drummond, J. P., Carpenter, M. H., and Riggins, D. W., Mixing and Mixing Enhancement in High Speed Reacting Flows. High Speed Flight Propulsion Systems, Chapter 7, Progress in Astronautics and Aeronautics, Vol. 137, 1991.

[3] Givi, P., and Riley, J. J., Some Current Issues in the Analysis of Reacting Shear Layers: Computational Challenges. Major Research Topics in Combustion, Editors: M. Y. Hussaini, A. Kumar and R. G. Voigt, pp. 588-650, Springer-Verlag, New York, NY, 1992.

[4] Drummond, J. P., and Givi, P., Suppression and Enhancement of Mixing in High-Speed Reacting Flow Fields. Combustion in High-Speed Flows, pp. 191- 229, Editors: J. Buckmaster, T. L. Jackson and A. Kumar, Kluwer Academic Publishers, Boston, MA, 1994.

[5] Goebel, S. G., and Dutton, J. C., Velocity Measurements of Compressible, Turbulent Mixing Layers. AIAA Paper 90-0709, January 1990.

[6] Hall, J. L., Dimotakis, P. E., and Rosemann, H., Experiments in Non-reacting Compressible Shear Layers. AIAA Paper 91-0629, January 1991.

[7] Sullins, G. A., Gilreath, H. E., Mattes, L. A., King, P. S., and Schetz, J. A., Instabilities in Confined Supersonic Mixing Layers. Tenth Int. Symposium on Air Breathing Engines, ISABE 91-7096, 1991.

[8] Samimy, M., Zaman, K. B. M .Q., and Reeder, M. F., Effect of Tabs on the Flow and Noise Field of an Axisymmetric Jet. AIAA Journal, Vol. 31, No. 4, pp. 609-619, 1993.

[9] Cox, S. K., Fuller, R. P., Schetz, J. A., and Walters, R. W., Vortical Interactions Generated by an Injector Array to Enhance Mixing in Supersonic Flow. AIAA Paper 94-0708, January 1994.

[10] Seiner, J. M., Dash, S. M., and Kenzakowski, D. C., Historical Survey on Enhanced Mixing in Scramjet Engines. AIAA Paper 99-4869, August 1999.

[11] Bogdanoff, D. W., Advanced Injection and Mixing Techniques for Scramjet Combustors. AIAA Journal of Propulsion and Power, Vol. 10, No. 2, pp. 183-190, 1994.

[12] Cutler, A. D., Harding, G. C., and Diskin, G. S., High Frequency Supersonic Pulsed Injection. AIAA Paper 2001-0517, January 2001.

[13] Schetz, J. A., Cox-Stouffer, S. K., and Fuller, R. P., Integrated CFD and Experimental Studies of Complex Injectors in Supersonic Flows. AIAA Paper 98-2780, June 1998.

[14] Cutler, A. D., Carty, A., Doerner, S., Diskin, G., and Drummond, J. P., Supersonic Coaxial Jet Flow Experiment for CFD Code Validation. AIAA Paper 99-3588, June 1999.

[15] Cutler, A. D., and White, J. A., An Experimental and CFD Study of a Supersonic Coaxial Jet. AIAA Paper 2001-0143, January 2001.

[16] Cutler, A., Danehy, P. M., Springer, R. R., and DeLoach, D. P., CARS Thermometry in a Supersonic Combustor for CFD Code Validation. AIAA Paper 2002-0743, January 2002.

[17] Drummond, J. P., Numerical Simulation of a Supersonic Chemically Reacting Mixing Layer. NASA TM 4055, 1988.

[18] Eggers, J. M., Turbulent Mixing of Coaxial Compressible Hydrogen-Air Jets. NASA TN D-6487, 1971.

[19] Eklund, D. R., et al., Computational/ Experimental Investigation of Staged Injection into a Mach 2 Flow. AIAA Journal, Vol. 32, No. 5, pp. 907-916, 1994.

[20] Carpenter, M. H., Three-Dimensional Computations of Cross-Flow Injection and Combustion in a Supersonic Flow. AIAA Paper 89-1870, June 1989.